Supporting Information for

Oxygen vacancy-regulated nanorod array electrodes for boosting the electrocatalytic synthesis of ammonia from nitrate wastewater

Ziyi Yang[a], Yudong Li[b], Dan Liu[b], Maosen Song[a], Yang Gao[a], Bin Yang[a], Yanzhen He[a,*],

Enshan Han[a], Qiang Zhang[c,d*], Xiaohui Yang[e,*]

a School of Chemical Engineering, Hebei University of Technology, Tianjin, 300400, China

b Key Laboratory of Bio-based Material Science & Technology, Northeast Forestry University, Ministry of Education, Harbin, 150040, China

c School of Chemistry & Chemical Engineering, Chongqing University of Technology, Chongqing 400054, P. R. China.

d National Engineering Laboratory for Methanol to Olefins, Dalian National Laboratory for Clean Energy, iChEM (Collaborative Innovation Center of Chemistry for Energy Materials), Dalian Institute of Chemical Physics, Chinese Academy of Sciences, Dalian 116023, P. R. China.

e Chongqing Institute of Green and Intelligent Technology, Chinese Academy of Sciences, Chongqing, 400714, China

*Corresponding authors.

E-mail addresses: yzhe87@163.com (YZ. He); zqiang@cqut.edu.cn (Q. Zhang) yangxiaohui@cigit.ac.cn (XH. Yang).

Mailing address for correspondence:

Qiang Zhang (A/Prof.)

School of Chemistry & Chemical Engineering, Chongqing University of Technology, Chongqing 400054, P. R. China.

E-mail: zqiang@cqut.edu.cn

Experimental section

Chemicals

Copper foam (CF), Sodium hydroxide (NaOH), Ammonium persulfate ($(NH_4)_2S_2O_8$), Ferrous sulfate ($FeSO_4$), Ammonium chloride (NH_4Cl), Sodium nitrate ($NaNO_3$), Sodium nitrite ($NaNO_2$), Sulfanilamide ($C_6H_8N_2O_2S$), N-(1-naphthyl) ethylenediamine dihydrochloride ($C_{12}H_{14}N_2 \cdot 2HCl$), potassium sodium tartrate ($NaKC_4H_4O_6$), sulfamic acid (HSO_3NH_2), urea ($CO(NH_2)_2$). Ethanol, hydrochloric acid, Phosphoric acid, Sulfuric acid, and Nessler Reagent were analytically pure and obtained from commercial suppliers. The copper foam (CF) was purchased from Tianjin Annohe New Energy Technology Co. LTD, China. Ultrapure water was applied to prepare the electrolyte solution.

Preparation of the $Cu(OH)_2$ Nanowires

The synthesis of 3D Cu/Fe_2O_3 nanorod arrays is schematically depicted in Figure 1a. Initially, 2 cm^2 copper foam (thickness: 1 mm, porosity: 97 %) was sonicated in 1 M hydrochloric acid for 20 min, then rinsed with amounts of ethanol and deionized water several times. Typically, the copper foam was placed in a solution containing 0.1 M $(NH_4)_2S_2O_8$ and 2 M NaOH for 20 min at room temperature. Then the sample was rinsed with ethanol and deionized water several times and dried in a vacuum at 70 °C for 6 h.

Preparation of the Cu/Fe_2O_3 Nanorod Arrays

The as-prepared $Cu(OH)_2$ nanowires on copper foam were immersed in $FeSO_4$ solution (5 mM) for 1, 7, 13, and 19 h, then rinsed with ethanol and deionized water several times and dried in vacuum at 70 °C overnight. Subsequently, the dried sample was loaded in a quartz boat and positioned at the center of a quartz tube. Following a 30-minute purge with Ar to eliminate O_2 from the quartz tube, the sample was

heated and maintained at 350 °C for 3 h with a heating rate of 5 °C min^{-1}. Afterward, the sample was allowed to cool down to room temperature naturally, resulting in the formation of black films on the copper foam. Then the catalysts Cu/Fe_2O_3-x (x=1, 7, 13, 19) were obtained by electroreduction performed at the current density of 20 mA cm^{-2}.

Sample Characterization

The X-ray diffraction (XRD) patterns were recorded on a Bruker D8 Focus diffractometer with Cu Kα radiation at 40 kV and 40 mA. Scanning electron microscope (SEM) images were carried out on Czech TESCAN MIRA LMS. X-ray photoelectron spectra (XPS) patterns were obtained on a Thermo Scientific K-Alpha X-ray photoelectron spectrometer with Al Kα radiation as the excitation source, the operating voltage was 12 kV. Transmission electron microscopy (TEM), energy spectrum surface scan (mapping), and high-resolution transmission electron microscopy (HR-TEM) images were taken on FEI Tecnai G2F 20. Electron paramagnetic resonance (EPR) spectra were taken on Bruker EMX PLUS. The isotope labeling experiments were measured by ^1H NMR measurement (JNM-ECZ600R). The ultraviolet-visible (UV-Vis) absorption spectra were tested on a Shimadzu UV-2600i spectrometer.

Electrochemical measurements

All electrochemical measurements were conducted on a CHI 660E electrochemical workstation (Chenhua, Shanghai) with a three-electrode system at room temperature. The electrolytic cell used in the experiment was a sealed single-chamber electrolytic cell. The prepared electrode sheet (1 cm^2) was used as the working electrode (cathode), saturated calomel electrode (SCE) was used as the reference electrode, and platinum plate (1 cm^2) was used as the opposite electrode (anode). Electrolyte solution (60 mL) was Ar-saturated of 0.2 M Na_2SO_4 with 100 ppm $NaNO_3$-N (NO_3^--N). Unless otherwise stated, the current density is normalized to the geometric area of the working electrode. Linear sweep voltammetry

(LSV) curves were performed at a scan rate of 10 mV s^{-1} from -0.2 to -1.6 V vs. SCE. The i-t tests were conducted at different potentials (-0.8, -1.0, −1.2, −1.4, -1.6, and -1.8 V vs. SCE) for 3 h with a stirring rate of 500 rpm. The EIS was recorded at 0.2 M Na_2SO_4 containing 100 ppm NO_3^--N with a frequency from 10^5 to 0.1 Hz, the test was performed at open-circuit potential with an amplitude of 0.005 V. The electrochemical double-layer capacitance (C_{dl}) method was used to calculate the electrochemical active surface areas (ECSA). Cyclic voltammetry (CV) curves were measured in a nonfaradaic region (from -0.05 to 0.05 V vs. SCE) at various scan rates (20, 40, 60, 80, and 100 mV s^{-1}) for determining C_{dl}. The capacitance $|j_a - j_b|/2$ was plotted against the scan rates to obtain the slope of the linear fitting equation, which represents C_{dl}. The ECSA value is equal to the C_{dl} divided by the specific capacitance (C_s=40 μF cm^{-2}). Nitrate, nitrite, and ammonium ion concentrations were measured by UV-Vis spectrophotometry, and more detailed information about the assay is available in the Supporting Information. Unless otherwise stated, all experiments were repeated twice to plot error bars.

Determination of NO_3^-

A certain amount of electrolyte was taken out from the cathode chamber and diluted to 25 mL with deionized water. The diluted electrolyte was mixed with 1 mL hydrochloric acid (1 M) and 0.1 mL HSO_3NH_2 solution (1.0 wt%). The mixture was stood for 20 min to ensure complete color development. The absorbance of the mixture was measured with UV-vis absorption spectrum at 220 nm and 275 nm. The concentration-absorbance curve was calibrated using a series of standard sodium nitrate solutions.

Determination of NO_2^-

A mixture of p-aminobenzene sulfonamide (4 g), N-(1-Naphthyl) ethylenediamine dihydrochloride (0.2 g), ultrapure water (50 mL), and phosphoric acid (10 mL, ρ= 1.70 g/mL) was

used as a color reagent. A certain amount of electrolyte was taken out from the cathode chamber and diluted to 25 mL with deionized water. Then, 0.1 mL color reagent was added into the aforementioned 25 mL solution and mixed uniformity, and the absorption intensity at a wavelength of 540 nm was recorded after sitting for 20 min. The concentration-absorbance curve was calibrated using a series of standard sodium nitrite solutions.

Determination of NH_4^+

A certain amount of electrolyte was taken out from the cathode chamber and diluted to 25 mL with deionized water. The diluted electrolyte was mixed with 1 mL Nessler Reagent and 1 mL $NaKC_4H_4O_6$ solution (500 g/L). The mixture was stood for 20 min to ensure complete color development. The absorbance of the mixture was measured with UV-vis absorption spectrum at 420 nm. The concentration-absorbance curve was calibrated using a series of standard ammonium chloride solutions.

Isotope labeling experiments

Isotope labeling experiments combined with the ^1H nuclear magnetic resonance (^1H NMR) technology were employed to identify the source of N in the product. The electrolyte was composed of 100 ppm $NaNO_3$ and 0.2 M Na_2SO_4. Before NitRR, high-purity Ar was continuously purged into the electrolytic cell for 20 min to remove impurity gas. After electrolysis at -1.4 V vs. SCE for 3 h, 5 mL of the electrolyte was taken out, and then acidized to pH~3. Afterward, the concentrated solution was mixed with dimethyl sulfoxide (DMSO) for ^1H NMR measurement.

Calculation of conversion efficiency

The NO_3^- conversion rate (η) was calculated by the following equation:

$$\eta(\%) = \frac{(c_0 - c_t)}{c_0}$$

The selectivity (S) of NO_2^- and NH_3 (NH_4^+) selectivity was calculated by the following equation:

$$NO_2^- - N(\%) = \frac{c_{NO_2^-}}{c_0 - c_t}$$

$$NH_4^+ - N(\%) = \frac{c_{NH_4^+}}{c_0 - c_t}$$

The NH_3 yield rate and faradic efficiency were calculated by the following equations:

$$NH_3\ \text{yield} = \frac{c_{NH_3} \times V}{M_{NH_3} \times t \times S}$$

$$FE_{NH_3} = \frac{8 \times F \times c_{NH_3} \times V}{M_{NH_3} \times Q}$$

Where c_0 is the initial Nitrate-N concentration, c_t is the concentration of Nitrate-N after reaction time t, c_{NH_3} is the measured average NH_3 mass concentration, $c_{NO_2^-}$ is the measured average NO_2^- mass concentration, V is the volume of the electrolyte (60 mL), M_{NH_3} is the molar mass of NH_3, t is the reaction time, S is the geometric area of working electrode (1 cm^2), F is the Faraday constant (96485 C mol^{-1}), Q is the total charge passed through the electrode.

Theoretical Simulation

We have employed the Vienna Ab Initio Package (VASP) to perform all the density functional theory (DFT) calculations within the generalized gradient approximation (GGA) using the PBE formulation. We have chosen the projected augmented wave (PAW) potentials to describe the ionic cores and take valence electrons into account using a plane wave basis set with a kinetic energy cutoff of 450 eV. Partial occupancies of the Kohn-Sham orbitals were allowed using the Gaussian smearing method and a width of 0.05 eV. The on-site corrections (DFT+U) have been applied to the 3d electron of Fe atoms (Ueff=5.3 eV) by the approach from Dudarev et al. The electronic energy was considered self-consistent when the energy change was smaller than 10^{-5} eV. A geometry

optimization was considered convergent when the force change was smaller than 0.02 eV/Å. Grimme's DFT-D3 methodology was used to describe the dispersion interactions.

The equilibrium lattice constants of the FCC-Cu unit cell were optimized a=3.569 Å. The equilibrium lattice constants of the hexagonal Fe_2O_3 unit cell were optimized a=5.024 Å, c=13.669 Å. We then use both to construct a Cu(220)/ Fe_2O_3(110) heterojunction surface model; The Fe_2O_3 (110) part has a p(1×3) periodicity in the X and Y directions and one stoichiometric layer in the Z direction; the Cu(220) part has a p(5×3) periodicity in the X and Y directions and 3 atomic layers in the Z direction; the whole slab was separated by vacuum depth of 15 Å in order to separate it from its periodic duplicates. During structural optimizations, a 1×2×1 in the Brillouin zone was used for k-point sampling, and the bottom two atomic layers of the Cu(220) part were fixed while the rest were allowed to fully relax.

Initially, the $Cu(OH)_2$ nanowires are prepared on copper foam, and the $Cu_2O/Fe(OH)_3$ nanorods are obtained by reaction with Fe^{2+} ionic solution through HCR reaction. The Fe^{2+} ions undergo initial hydrolysis, resulting in the deposition of $Fe(OH)_3$ on the $Cu(OH)_2$ nanowires/solution interface. The growth of $Fe(OH)_3$ on $Cu(OH)_2$ nanowires likewise increases due to prolonged HCR reaction times, thus the concentration of oxygen vacancies is artificially controlled during this process (Fig. S1). This process also leads directly to the release of H^+ ions, generating an acidic environment. Subsequently, Fe^{2+} ions undergo a redox reaction with $Cu(OH)_2$ nanowires in an acidic solution. Interestingly, in the acidic solution, the reduction ability of Fe^{2+} ions is significantly enhanced in the acidic solution, leading to the reduction of in-situ $Cu(OH)_2$ nanowires array and the formation of Cu_2O nanorods core cubic phase embedded within the $Fe(OH)_3$ shell. This phase is denoted as $Cu_2O/Fe(OH)_3$. Subsequently, $Fe(OH)_3$ was pyrolyzed to Fe_2O_3 at high temperatures, and Cu_2O was reduced to Cu by receiving electrons at the cathode. The reactions are demonstrated in Eqs. (1-4):

$$Cu + 4NaOH + (NH_4)_2S_2O_8 \rightarrow Cu(OH)_2 + 2Na_2SO_4 + 2NH_3 + 2H_2O \quad (1)$$

$$2Fe^{2+} + 3H_2O + 2Cu(OH)_2 \rightarrow 2Fe(OH)_3 + Cu_2O + 4H^+ \quad (2)$$

$$Cu_2O + 2e^- + 2H^+ \rightarrow Cu + H_2O \quad (3)$$

$$2Fe(OH)_3 \rightarrow Fe_2O_3 + 3H_2O \quad (4)$$

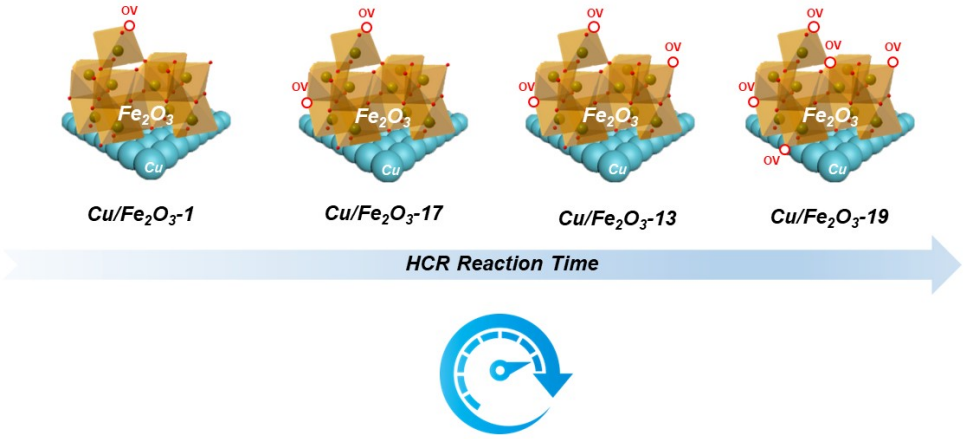

Fig. S1. Model diagram of samples.

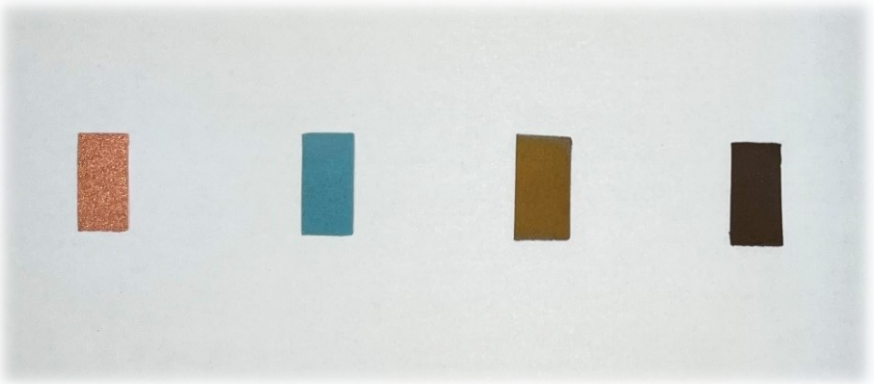

Fig. S2. Optical image illustrating the color evolution from Cu foam to the 3D Cu/Fe_2O_3 nanorod array.

The optical image in Fig. S2 shows the color evolution from Cu foam to the 3D Cu/Fe_2O_3 nanorods array film grown on the copper foam. The color of the copper substrate surface changes from brassy metal (Cu), blue ($Cu(OH)_2$), yellow ($Cu_2O/Fe(OH)_3$), to black (Cu/Fe_2O_3).

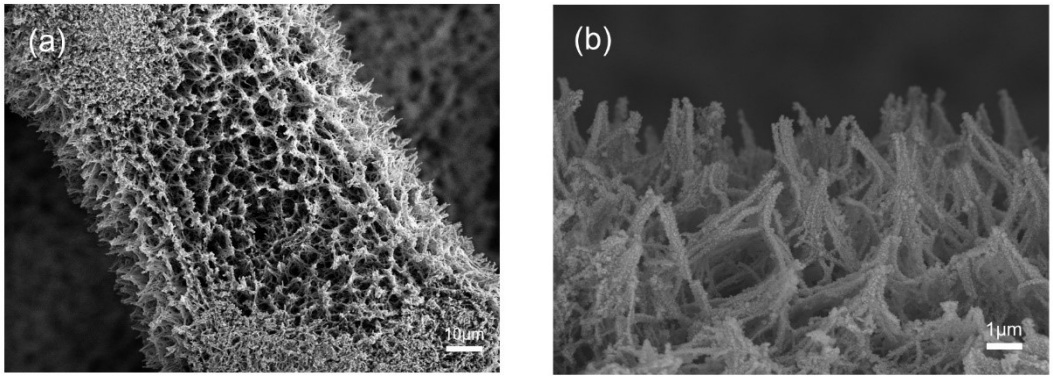

Fig. S3. SEM images of Cu/Fe_2O_3-13 after 3h NitRR.

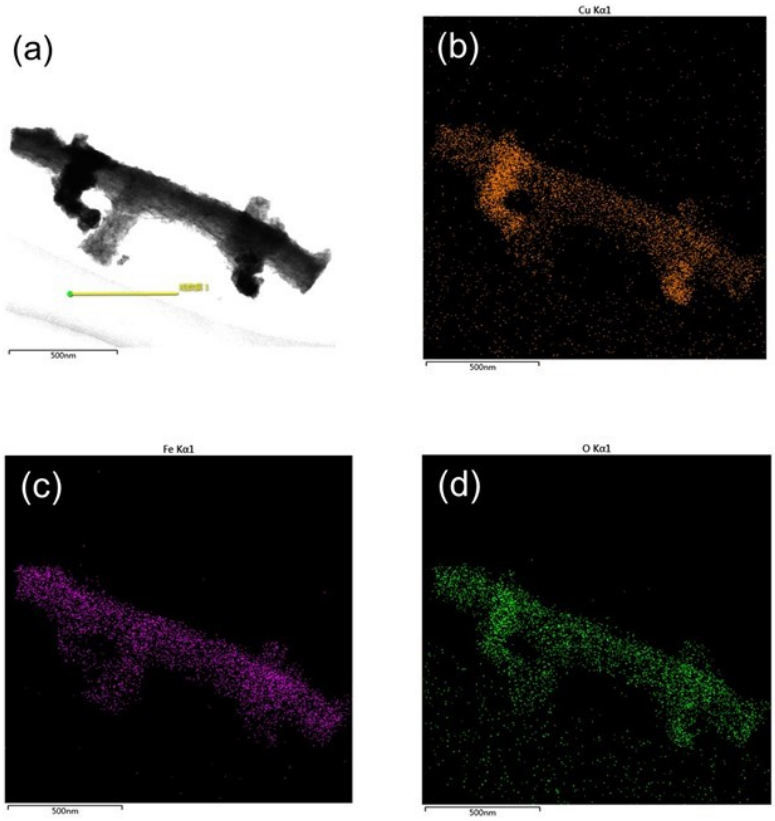

Fig. S4. (a) TEM image and (b-d) elemental mapping images of Cu/Fe_2O_3-13 after 3h NitRR.

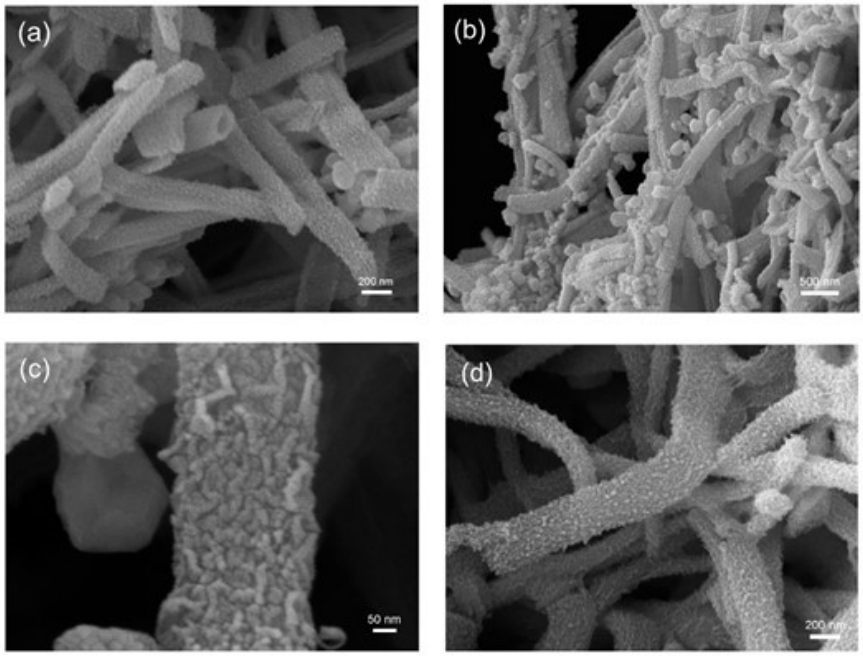

Fig. S5. SEM images of (a) Cu/Fe_2O_3-1, (b) Cu/Fe_2O_3-7, (c) Cu/Fe_2O_3-13, and (d) Cu/Fe_2O_3-19 nanorods array on copper foam.

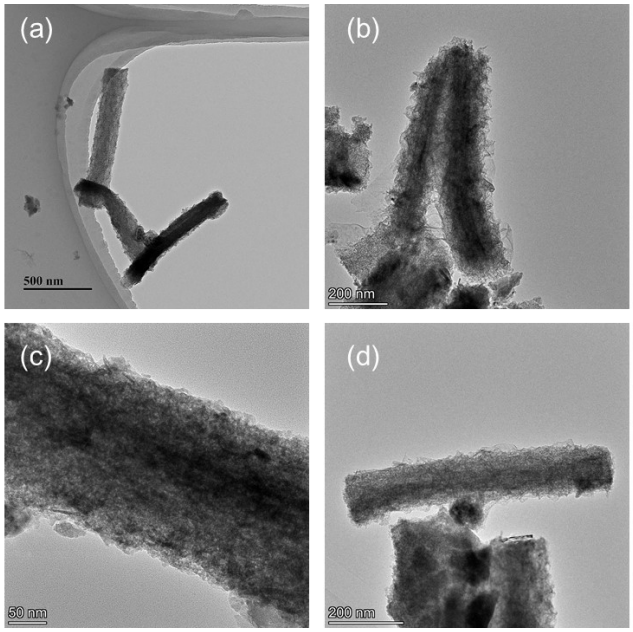

Fig. S6. TEM images of Cu/Fe_2O_3-13.

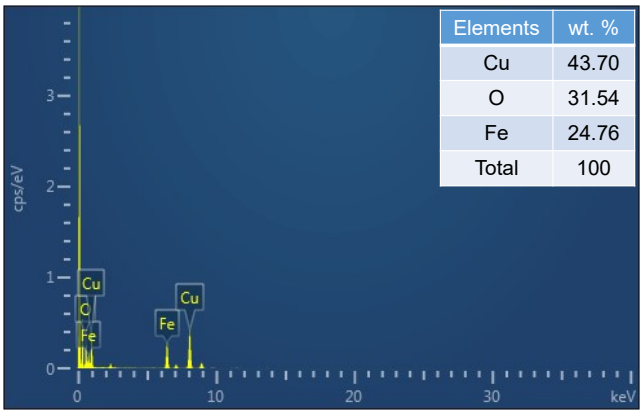

Fig. S7. TEM-EDX spectrum of elements for a single Cu/Fe_2O_3-13 nanorod.

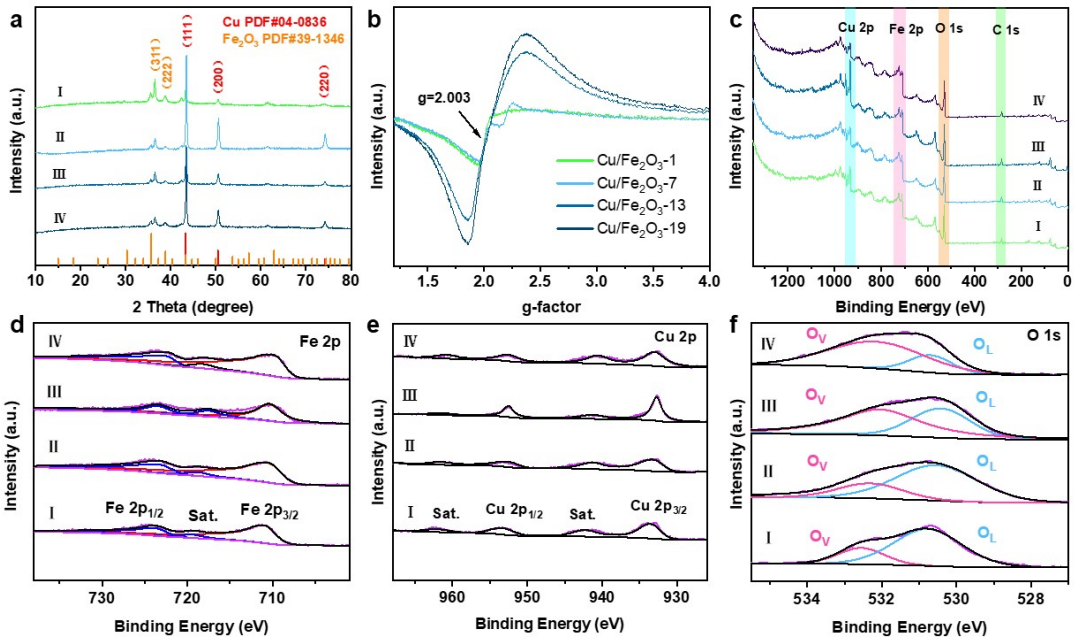

Fig. S8. (a) XRD pattern, (b) EPR spectra, (c) XPS survey spectra, high-resolution XPS spectra of (d) Fe 2p, (e) Cu 2p, and (f) O 1s for I) Cu/Fe_2O_3-1, II) Cu/Fe_2O_3-7, III) Cu/Fe_2O_3-13, and IV) Cu/Fe_2O_3-19.

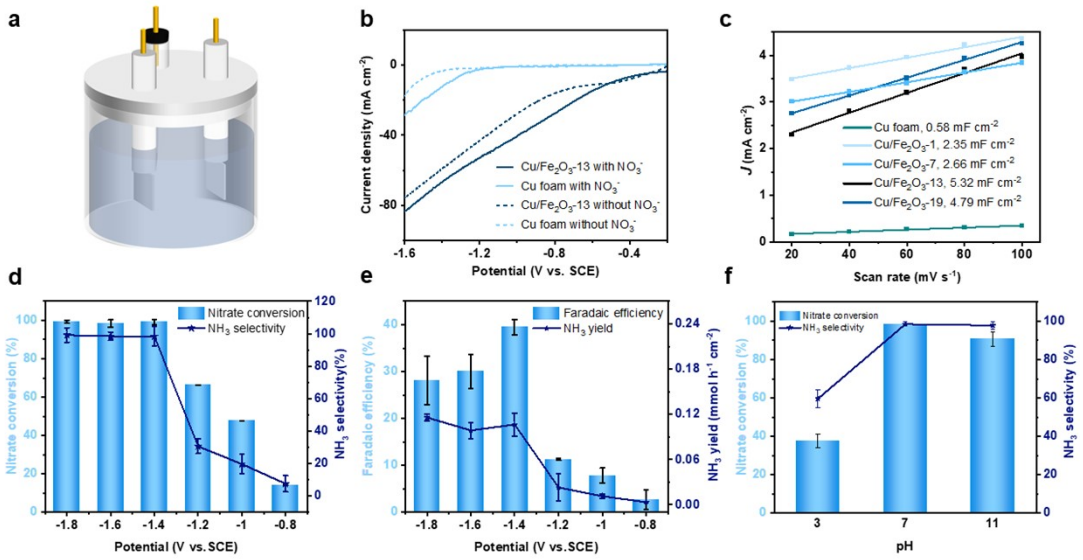

Fig. S9. (a) Schematic illustration of the test device for the NitRR. (b) LSV curves of Cu/Fe_2O_3-13 and Cu foam. (c) The electrochemical double-layer capacitors of samples. (d) Nitrate conversion and NH_3 selectivity of Cu/Fe_2O_3-13 at different potentials. (e) FE and NH_3 yield of Cu/Fe_2O_3-13 at different potentials. (f) Nitrate conversion and NH_3 selectivity for Cu/Fe_2O_3-13 in electrolytes with different pH values.

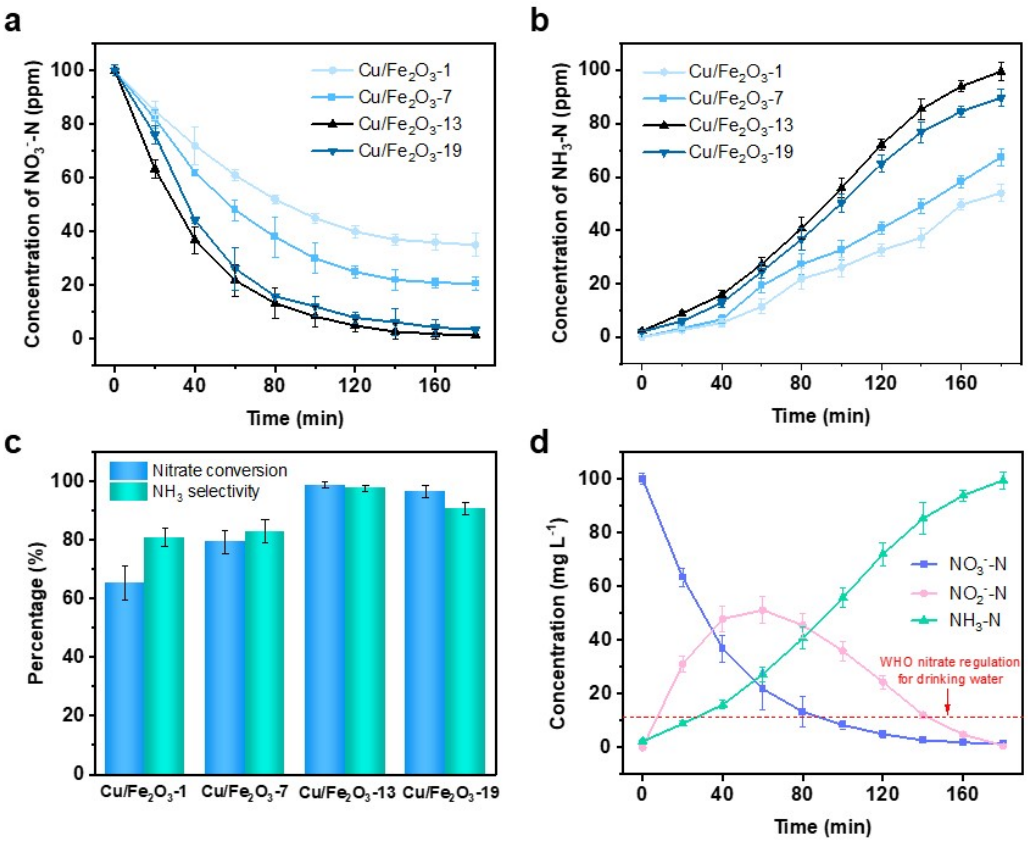

Fig. S10. Time-Dependent concentrations of (a) NO_3^--N and (b) NH_4^+-N for Cu/Fe_2O_3-1, Cu/Fe_2O_3-7, Cu/Fe_2O_3-13, and Cu/Fe_2O_3-19 at -1.4 V vs. SCE. (c) Nitrate conversion and NH_3 selectivity for Cu/Fe_2O_3-1, Cu/Fe_2O_3-7, Cu/Fe_2O_3-13, and Cu/Fe_2O_3-19 at -1.4 V vs. SCE. (d) Time-Dependent concentrations of $^{NO_3^-}$-N, $^{NO_2^-}$-N, and $^{NH_4^+}$-N over Cu/Fe_2O_3-13.

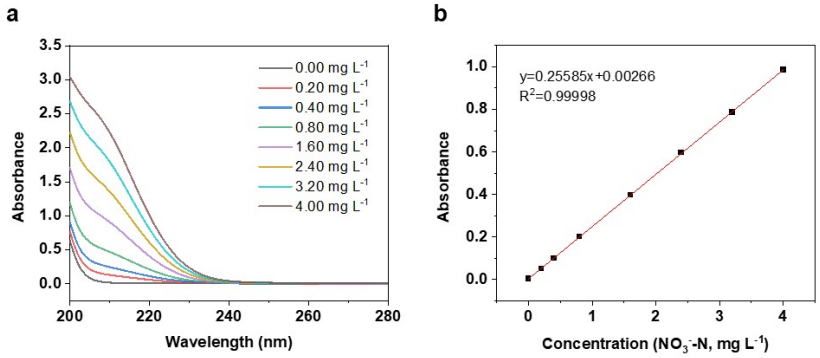

Fig. S11. (a) UV-Vis absorption spectra of the NO_3^--N standard solution with different concentrations. (b) Calibration curve of NO_3^--N for evaluating nitrate conversion efficiency.

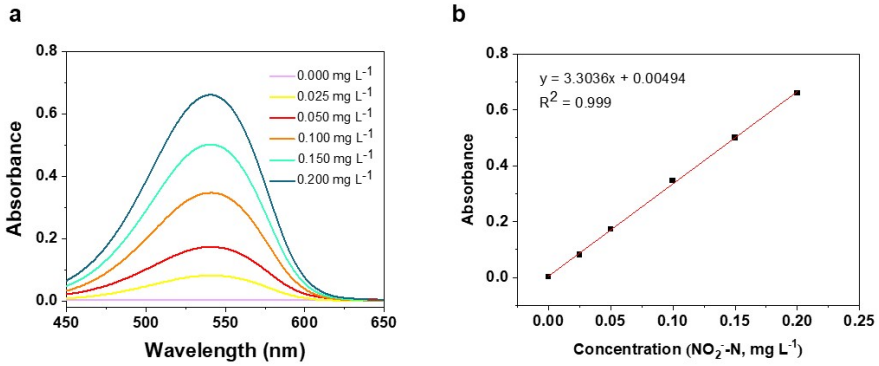

Fig. S12. (a) UV-Vis absorption spectra of the NO_2^--N standard solution with different concentrations. (b) Calibration curve of NO_2^--N for evaluating nitrate conversion efficiency.

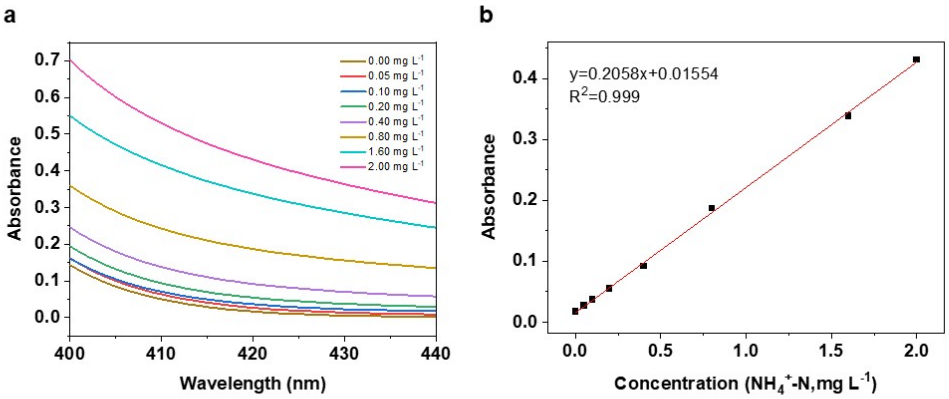

Fig. S13. (a) UV-Vis absorption spectra of the NH_4^+-N standard solution with different concentrations. (b) Calibration curve of NH_4^+-N for evaluating nitrate conversion efficiency.

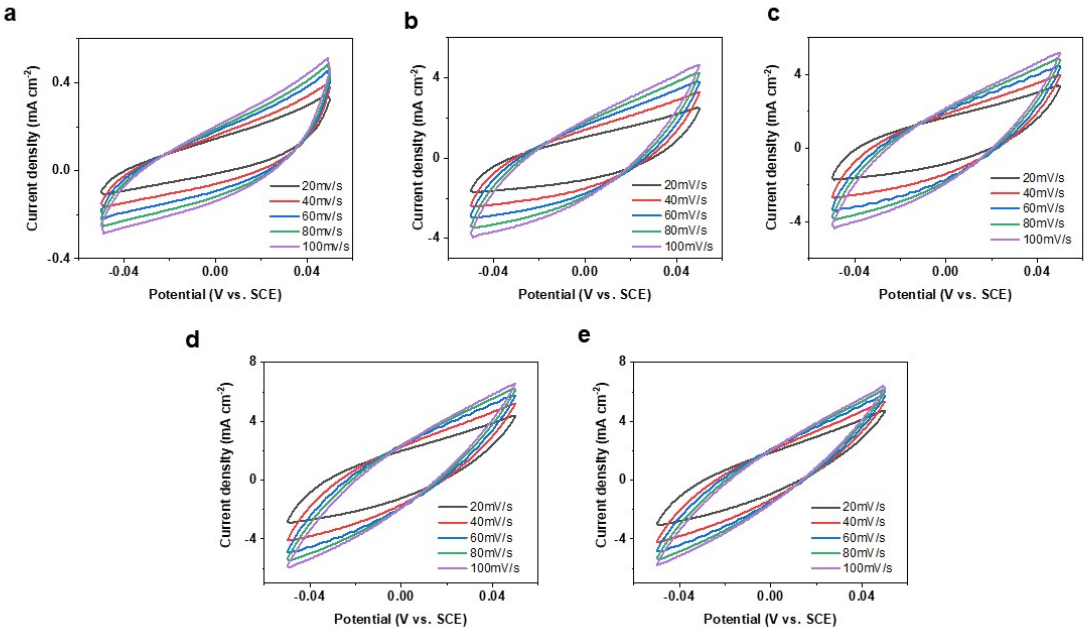

Fig. S14. Cyclic voltammetry curves of (a) Cu foam, (b) Cu/Fe_2O_3-1, (c) Cu/Fe_2O_3-7, (d) Cu/Fe_2O_3-13, and (e) Cu/Fe_2O_3-19 at various rates (20, 40, 60, 80 and 100 mV s^{-1}).

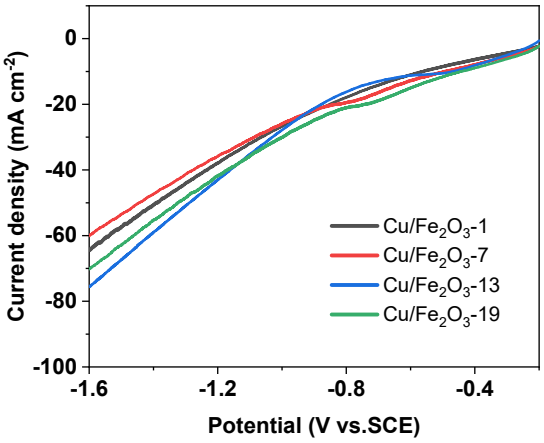

Fig. S15. The normalized LSV curves of Cu/Fe_2O_3-1, Cu/Fe_2O_3-7, Cu/Fe_2O_3-13, and Cu/Fe_2O_3-19.

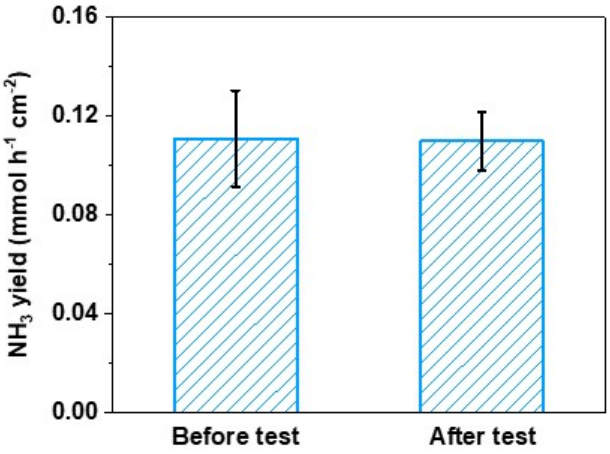

Fig. S16. Ammonia yield of Cu/Fe_2O_3-13 before and after the long-term potentiostat experiment.

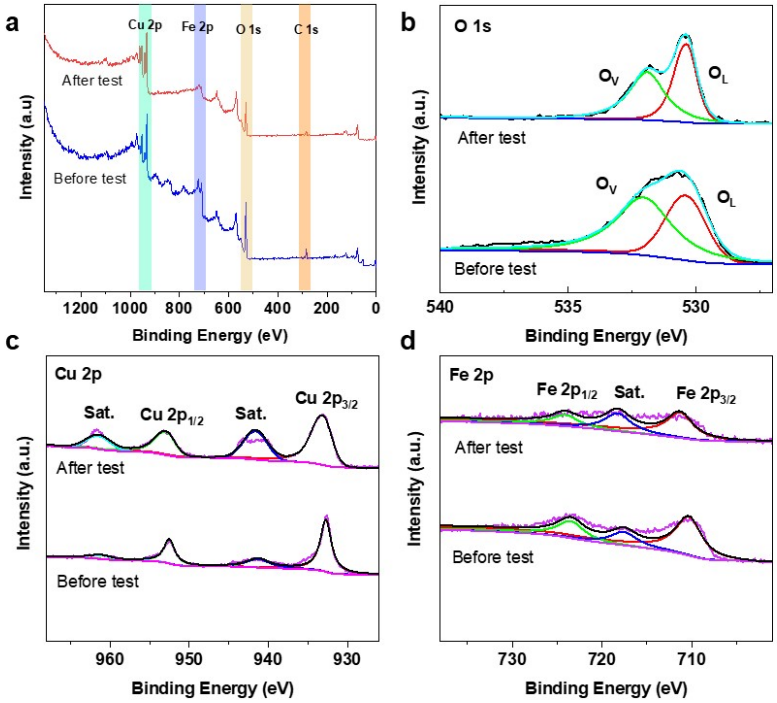

Fig. S17. (a) X-ray photoelectron survey spectra, (b) O 1s, (c) Cu 2p, and (d) Fe 2p spectra of the 3D Cu/Fe_2O_3-13 nanorod array electrode before and after the cyclic test.

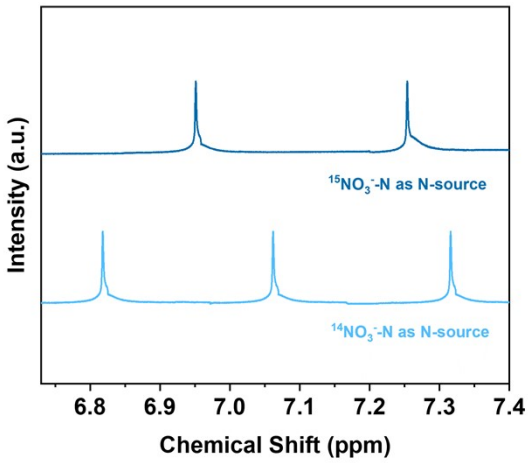

Fig. S18. ^{1}H NMR spectra of the electrolyte while using $^{15}NO_3^-$-N and $^{14}NO_3^-$-N as the nitrogen sources.

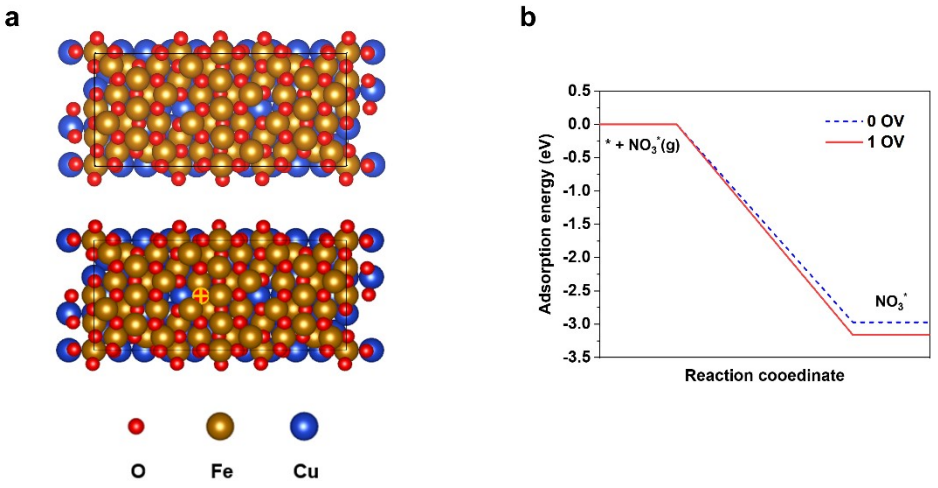

Fig. S19. (a) Top view of the Cu(220)/Fe_2O_3(110) atomic configuration without the OV (Top) and with the OV (Bottom, Note: the yellow plus sign indicates the oxygen vacancy position); (b) The calculated adsorption energies of NO_3^- ions on the Cu(220)/Fe_2O_3(110) surfaces with and without OV.

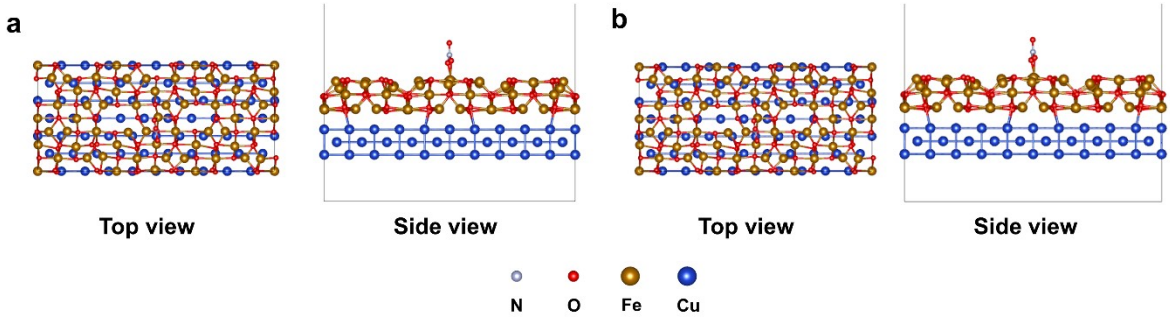

Fig. S20. (a) Top (left) and side (right) views of the Cu(220)/Fe_2O_3(110) adsorption configuration without oxygen vacancy; (b) Top (left) and side (right) views of the adsorption configuration of Cu(220)/Fe_2O_3(110) with oxygen vacancy.

In the direct reduction process, the adsorbed NO_3^-(ad) is first reduced to NO_3^{2-}(ad) by electrons at the electrode, which is usually considered the rate-limiting step. Subsequently, NO_3^{2-}(ad) is reduced to NO_2^-(ad), which is further reduced to NH_3 after gaining electrons. The reactions are demonstrated in Eqs. (5-9):

$$NO_{3\,(aq)}^- \rightarrow NO_{3\,(ad)}^- \quad (5)$$

$$NO_{3\,(ad)}^- + e^- \rightarrow NO_{3\,(ad)}^{2-} \quad (6)$$

$$NO_{3\,(ad)}^{2-} + 2H^+ + e^- \rightarrow NO_{2\,(ad)}^- + H_2O \quad (7)$$

$$NO_{2\,(ad)}^- + 4H^+ + 3e^- \rightarrow H_2NO_{(ad)} + H_2O \quad (8)$$

$$H_2NO_{(ad)} + 3H^+ + 3e^- \rightarrow NH_3 + H_2O \quad (9)$$

This process consists of H* acting as a reducing agent. The reactions are demonstrated in Eqs. (10-13):

$$NO_{3\,(ad)}^- + 2H^* \rightarrow NO_{2\,(ad)}^- + H_2O \quad (10)$$

$$NO_{2\,(ad)}^- + H^* \rightarrow NO_{(ad)} + OH^- \quad (11)$$

$$NO_{(ad)} + 2H^* \rightarrow N_{(ad)} + H_2O \quad (12)$$

$$N_{(ad)} + 3H^* \rightarrow NH_3 \quad (13)$$

Table S1. Comparison of nitrate conversion and generated NH_3 selectivity of Cu/Fe_2O_3-13 in this work with other materials reported in recent studies.

Electrocatalyst	Operating conditions	Nitrate conversion	NH_3 selectivity	Ref.
Cu/Fe_2O_3-13	100 ppm NO_3^--N + 0.2 M Na_2SO_4, -1.4 V vs. SCE	99.10%	98.30%	This work
Cu/Cu_2O NWAs	200 ppm NO_3^--N + 0.5 M Na_2SO_4, -0.85 V vs. RHE	97.0%	81.2%	(Wang et al., 2020)
Cu_3P/CF	50 ppm NO_3^--N + 1500 ppm NaCl, -1.23 V vs. Ag/AgCl	84.3%	2.2%	(Yao et al., 2021)
CuPd(3 : 1)	50 ppm NO_3^--N + 0.5 M K_2SO_4, -0.3 V vs. RHE	95.27%	77.49%	(Xu et al., 2021)
Cu-Bi	100 ppm NO_3^--N + 0.1 M Na_2SO_4, 6 mA cm^{-2}	87.5%	19%	(Gao et al., 2018)
FeNi/g-mesoC/NF	50 ppm NO_3^--N + 0.05 M Na_2SO_4, -1.3 V vs. SCE	88%	64.2%	(Chen et al., 2020)
CuFe NPs@N-C/NF	50ppm NO_3^- + 50mM SO_4^{2-}, -1.4 V vs. Ag/AgCl	75.2%	94.0%	(He et al., 2023)
Cu/Fe@NCNFs	100ppm NO^{3-} + 0.1M Na_2SO_4, -1.3V vs. RHE	76%	94%	(Lan et al., 2021)

References

1. Chen, X., Zhang, T., Kan, M., Song, D., Jia, J., Zhao, Y., Qian, X., 2020. Binderless and Oxygen Vacancies Rich FeNi/Graphitized Mesoporous Carbon/Ni Foam for Electrocatalytic Reduction of Nitrate. Environ. Sci. Technol. 54(20), 13344-13353.
2. Gao, W., Gao, L., Li, D., Huang, K., Cui, L., Meng, J., Liang, J., 2018. Removal of nitrate from water by the electrocatalytic denitrification on the Cu-Bi electrode. J. Electroanal. Chem. 817, 202-209.
3. He, L., Zeng, T., Yao, F., Zhong, Y., Tan, C., Pi, Z., Hou, K., Chen, S., Li, X., Yang, Q., 2023. Electrocatalytic reduction of nitrate by carbon encapsulated Cu-Fe electroactive nanocatalysts on Ni foam. J. Colloid Interface Sci. 634, 440-449.
4. Lan, Y., Luo, H., Ma, Y., Hua, Y., Liao, T., Yang, J., 2021. Synergy between copper and iron sites inside carbon nanofibers for superior electrocatalytic denitrification. Nanoscale 13(22), 10108-10115.
5. Wang, Y., Zhou, W., Jia, R., Yu, Y., Zhang, B., 2020. Unveiling the Activity Origin of a Copper-based Electrocatalyst for Selective Nitrate Reduction to Ammonia. Angew. Chem. Int. Ed. 59(13), 5350-5354.
6. Xu, Y., Ren, K., Ren, T., Wang, M., Liu, M., Wang, Z., Li, X., Wang, L., Wang, H., 2021. Cooperativity of Cu and Pd active sites in CuPd aerogels enhances nitrate electroreduction to ammonia. Chem. Commun. 57(61), 7525-7528.
7. Yao, F., Jia, M., Yang, Q., Chen, F., Zhong, Y., Chen, S., He, L., Pi, Z., Hou, K., Wang, D., Li, X., 2021. Highly selective electrochemical nitrate reduction using copper phosphide self-supported copper foam electrode: Performance, mechanism, and application. Water Res. 193, 116881.